We are IntechOpen, the world's leading publisher of Open Access books
Built by scientists, for scientists

6,900
Open access books available

186,000
International authors and editors

200M
Downloads

Our authors are among the

154
Countries delivered to

TOP 1%
most cited scientists

12.2%
Contributors from top 500 universities

CLARIVATE ANALYTICS
BOOK CITATION INDEX
INDEXED

WEB OF SCIENCE™

Selection of our books indexed in the Book Citation Index in Web of Science™ Core Collection (BKCI)

Interested in publishing with us?
Contact book.department@intechopen.com

Numbers displayed above are based on latest data collected.
For more information visit www.intechopen.com

5

New Neurostimulation Strategy and Corresponding Implantable Device to Enhance Bladder Functions

Fayçal Mounaïm and Mohamad Sawan
Polystim Neurotechnologies Laboratory, Department of Electrical Engineering
École Polytechnique de Montréal
Canada

1. Introduction

Spinal cord injury (SCI) is one of the most complex and devastating medical conditions. Its worldwide incidence ranges from 11 to 112 per 100,000 Population (Blumer & Quine, 1995; DeVivo, 1997). SCI leads to different degrees of dysfunction of the lower urinary tract due to a large variety of possible lesions. Immediately after SCI, flaccid paralysis sets in, followed by the absence of reflexes and a complete loss of sensory and motor control below the level of lesion, rendering the urinary bladder areflexic and atonic. This period, termed spinal shock, can extend from a few days to several months (Chai & Steers, 1996). Most patients with suprasacral SCI suffer from detrusor over-activity (DO) and detrusor sphincter dyssynergia (DSD) (Blaivas et al., 1981). DSD leads to high intravesical pressure, high residual urine, urinary tract infection, and deterioration of the upper urinary tract. In order to recover the voluntary control of micturition, functional electrical stimulation (FES) has been investigated at different sites of the urinary system: the bladder muscle (detrusor), the pelvic nerves, the spinal cord and the sacral nerve roots. Among these, sacral nerve root stimulation is considered the most efficient technique to induce micturition and has been prevalent in clinical practice over the last two decades (Elabaddy et al., 1994). Using cuff-electrodes, this technique offers the advantages of a safe and stable fixation of electrodes as well as confinement of the spread of stimulation current within the targeted nerves. However, the detrusor and the external urethral sphincter (EUS) muscles share the sacral nerves as common innervations pathways, and stimulation of the entire sacral root induces contraction of both. Thus, the efficiency of micturition by means of sacral neurostimulation depends on the capability to contract the detrusor without triggering EUS contraction. In order to improve this neurostimulation selectivity, several techniques have been proposed, among which are rhizotomy, and EUS blockade using high-frequency stimulation.

Dorsal rhizotomy consists of selectively severing afferent sacral nerve roots that are involved in pathological reflex arc in suprasacral SCI patients. Rhizotomy abolishes DO, reduces DSD, and prevents autonomic dysreflexia. As a beneficial result, the uninhibited bladder contractions are reduced, the bladder capacity and compliance are increased, urine flow is improved, and consequently the upper urinary tract is protected from ureteral reflux and hydronephrosis. In case of a complete SCI, dorsal rhizotomy is combined with an

implantable sacral ventral root stimulator such as the Finetech-Brindley Bladder System (also known as the VOCARE in North America) (Kutzenberger, 2007). In fact, this neurostimulation system is the only commercialized and FDA-approved solution aiming for micturition in SCI patients (Jezernik et al., 2002). Unfortunately, rhizotomy being irreversible, it has a fundamental disadvantage which is the abolition of sexual and defecation reflexes, as well as sacral sensations if still present in case of incomplete SCI.

High-frequency stimulation can be used to inhibit the contraction of the EUS muscle. However, the mechanism by which the EUS inhibition is obtained is not well understood and three explanations are possible: high-frequency stimulation may stop the propagation of nerve action potentials, may maintain the motor end-plate (neuromuscular junction) in a refractory status, or may fatigue the aimed muscle (Kilgore & Bhadra, 2004; Tai et al., 2005; Williamson & Andrews, 2005). Frequencies from 300 Hz to 30 kHz can be used to achieve a complete and reversible nerve conduction block depending on the stimulation amplitude (Solomonow, 1984; Sievert et al., 2002; Schuettler et al., 2004; Bhadra et al., 2006). However, below 1 kHz, a sinusoidal stimulation can generate action potentials at the same or a submultiple rate. Increasing the frequency has the advantage of lowering the amount of injected charge per-phase needed for a complete blockade. A graded blockade can also be achieved as blockade of each axon within the nerve is influenced by its diameter and the stimulation amplitude (Tai et al., 2005). If a graded blockade is applied distally in combination with low-frequency stimulation, selectivity with respect to axon diameter can be obtained by adjusting stimulation amplitude (Williamson & Andrews, 2005). Finally, combining sacral root stimulation with bilateral high-frequency pudendal nerve block led to effective micturition in male cats (Boger et al., 2008).

The efficiency of high-frequency blockade was studied with dog experiments using a neurostimulator designed by Polystim Neurotechnologies Laboratory (Robin et al., 1998; Shaker et al., 1998; Ba et al., 2002; Sawan et al., 2008b). The Polystim's stimulator generated a rectangular waveform combining two frequencies (e.g. 600 Hz and 30 Hz). It is important to point out in this case, that stimulation and blockade are both applied simultaneously at the same nerve site, with the same bipolar electrode. According to Kilgore et al. (Kilgore & Bhadra, 2004), blockade at 600 Hz frequency with less than 2 mA current is probably due to a muscle fatigue mechanism rather than nerve conduction blockade. The same neurostimulator was also implanted in paraplegic dogs for chronic experiments where it was demonstrated that the combination of low and high frequency stimuli resulted in 45 % reduction in EUS activity and that urine evacuation improved up to 91 % of the mean bladder capacity during the six months of chronic stimulation (Abdel-Gawad et al., 2001). The latest Polystim's neurostimulation prototypes using that stimulation strategy were UroStim6 and UroStim7 presented in (Mounaim et al., 2006; Mounaim & Sawan, 2007) respectively.

This chapter first describes a new sacral neurostimulation strategy to enhance micturition, based on nerve conduction blockade using high frequency stimulation as an alternative to rhizotomy. In order to test this strategy in chronic animal experiments, an implantable neurostimulation device is required. Thus, this chapter presents the design, test, prototyping and encapsulation of such neurostimulator (UroStim8) implementing the proposed stimulation strategy and using only commercially available discrete components.

2. New stimulation strategy

The proposed multi-site sacral neurostimulation strategy is illustrated in Fig. 1 and based on the following: High-frequency stimulation with an alternating waveform (such as sinusoidal

or rectangular) and optimum parameters, induces a blockade of the nerve (motor and/or sensory) activity, that may be complete (all axons) or partial (large diameter axons only). With a complete nerve blockade, the effect would be equivalent to that of rhizotomy while being controlled and totally reversible. With a partial blockade, selective stimulation can be achieved by blocking large axons only.

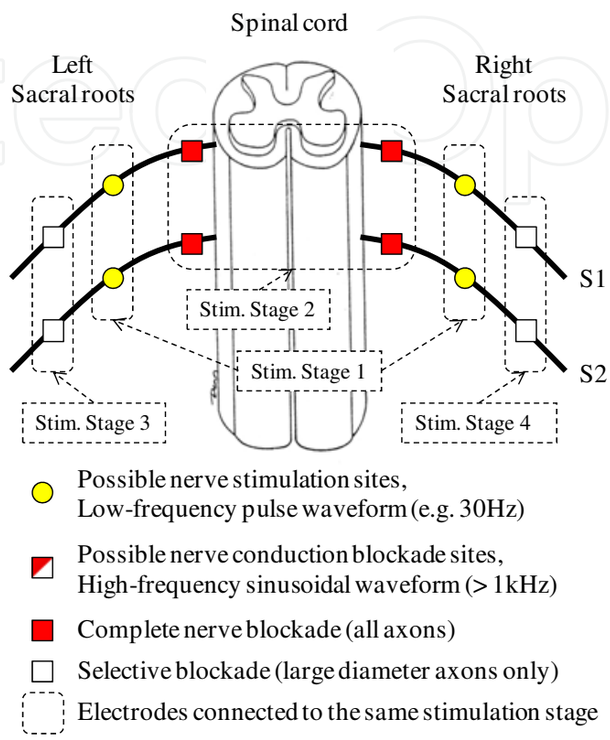

Fig. 1. Proposed multi-sites sacral neurostimulation strategy (dog model)

In order to induce a contraction of the detrusor, a low-frequency (e.g. 30 Hz) pulse current stimulation is applied to S2 sacral nerve(s) (or S1 eventually), unilaterally or bilaterally. Adjusting the stimulation pulse amplitude and width, the degree of contraction can be modulated. In most cases, the EUS contracts as well. The stimulation-evoked EUS contraction may be explained by direct and/or reflex mechanisms due to efferent and/or afferent fibers activation respectively. Both types of EUS activation can be avoided by blocking axons innervating the EUS muscle with high-frequency (> 1 kHz) stimulation. A selective blockade can be applied distally (between the low-frequency stimulation site and the EUS) to inhibit direct EUS activation, while a complete blockade can be applied proximally (between the low-frequency stimulation site and the spinal cord), to inhibit reflex EUS activation. However, reflex EUS activation may involve sacral root(s) other than the one(s) stimulated by the low-frequency waveform. In such case, they should be blocked as well. Anatomically, the lower urinary tract innervations are the same from one animal to another but there is a functional variability. It is possible that one type of EUS activation mechanisms is dominant. For illustration purposes, Fig. 1 shows all possible blockade sites, but it is also possible that one blockade site prove to be sufficient. In case of incomplete SCI, conventional sacral nerve stimulation may lead to pain perception. Rhizotomy can be a way to abolish the stimulation-evoked pain but will probably not be considered at the cost of

losing important reflexes and sensations if still present. With the proposed stimulation strategy, a complete proximal high-frequency blockade of sensory activity during low-frequency stimulation can inhibit pain sensation as well. Polystim Lab. recently presented preliminary results obtained with this strategy based on a dog model. Acute dog experiments were carried out and EUS blockade has been achieved in 8 animals after spinal cord transection (Mounaim et al. 2008; 2010). However, such experiments are not sufficient to validate the strategy especially that spinal shock generally lasts several weeks after SCI. Chronic experiments are mandatory in order to evaluate the long-term efficiency. This obviously requires a custom implantable neurostimulator that implements the proposed strategy, and will be capable of generating conventional stimulation waveforms as well as high-frequency sinusoids simultaneously over multiple channels.

3. Discrete implantable neurostimulator

3.1 Neurostimulator architecture

The block diagram of Fig.2 illustrates the architecture of the implantable neurostimulator UroStim8 dedicated to the new stimulation strategy. The neurostimulator has been designed with commercially available off-the shelf components. The control unit is one of the latest generation of Field Programmable Gate Arrays (FPGA) that presents advantageous low-power and small-scale features (Igloo, ACTEL). This FPGA also offers an In-Sytem Programming (ISP) feature that would allow (wired) subsequent code updates even after encapsulation of the neurostimulator. Such option was not possible with anti-fuse FPGAs used in previous prototypes (Ex, ACTEL) leading to the assembly of a new prototype for each new code to be tested. With near-field inductive coupling of spiral antennas, energy and data are wirelessly transmitted through the skin to the implanted stimulator using an external controller. The inductive coupling frequency used in previous prototypes was 20 MHz, but to comply with the Industrial, Scientific and Medical (ISM) radio band, it is reduced to 13.56 MHz. This frequency is chosen taking into account the coupling attenuation through the skin tissues and the spiral inductors characteristics. The Power Recovery stage rectifies and filters the inductive carrier signal to provide different regulated power supplies to the stimulator. The Data Recovery stage demodulates the 600 kHz On-Off Keying (OOK) modulated carrier to provide Manchester-coded data to the FPGA. As soon as the inductive energy is present and the power supply sufficient, the FPGA starts Manchester decoding to extract data at 300 Kbps and a synchronized clock at 300 kHz. Transmission data frames are sent cyclically until the FPGA acknowledges that a valid one is received without errors using a low power and short-range 1 kbps RF uplink at 433 MHz. Depending on the received instruction and parameters, a specific mode is executed. This could be a stimulation mode where one or multiple Stimulation Stages outputs can be activated with chosen parameters, or a telemetry mode where impedance module and phase of each electrode-nerve interface (ENI) can be measured at a chosen frequency. Even though all stimulation stages are similar and can generate any waveform to a certain extent, Stimulation Stage 1 is dedicated to the low-frequency pulse waveform while Stages 2 to 4 are dedicated to the high-frequency sinusoidal waveform. The stimulation frequency is common to Stages 2 to 4 but the stimulation current amplitude can be adjusted independently. The synchronized clock extracted from the Manchester-coded data was used as a time base for stimuli generation in previous neurostimulators. However, this clock suffers from time jitter due to inductive noise during data demodulation. Timing is very

important as for conventional biphasic stimulation for example, positive and negative phases must have the same duration so that total charge injection into the ENI is null. The oscillator in Fig. 2 is a low power component that brings a simple solution to this problem. Frequency of oscillation is adjusted with one resistance and an internal divider setting. The oscillator is activated for stimuli generation only and provides a stable clock of 300 kHz that can be eventually increased or decreased (hardware modification, not through the FPGA) depending on the available inductive power and the desired stimulation parameters.

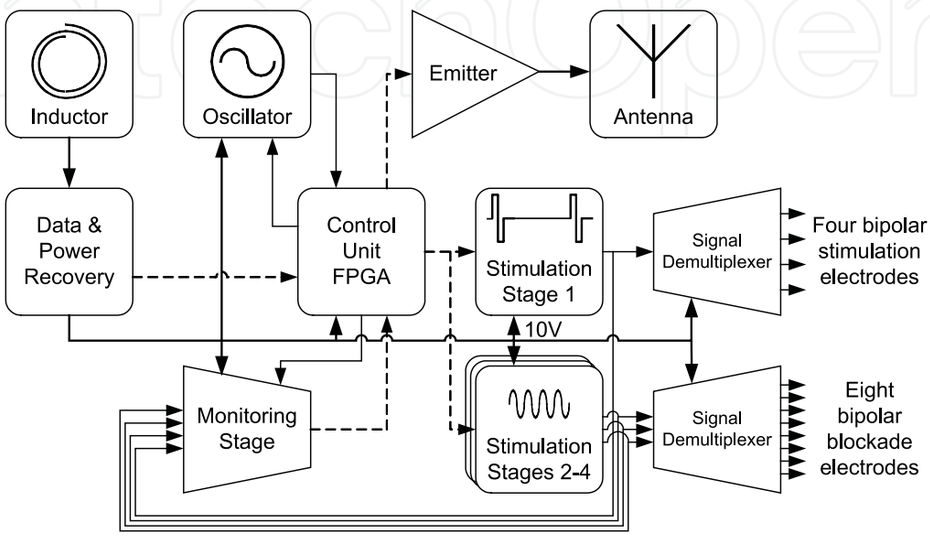

Fig. 2. Architecture of the UroStim8 neurostimulator dedicated to the new strategy

3.2 Power and data recovery

The neurostimulator front-end is responsible for power and data recovery as shown in Fig.3. Inductive energy transmitted by the external controller is recovered by the implanted stimulator using a parallel LC network resonating at the same frequency. Inductance L is a 3-turn spiral antenna that is printed on a thin and flexible PCB with external diameter of less than 4 cm and a trace width of 1 mm to reduce the series resistance. Capacitance C is made of parallel combinations of ceramic NPO capacitors that offer high Q and high temperature stability. The capacitors are also specified for 100 V in order to maintain acceptable values at high voltages and high frequency. C_{tune} is a miniature variable capacitor that allows fine tuning of the resonant frequency to recover maximum energy with respect to the average power consumption of the implant. The voltage across the resonating LC network is an alternating signal that may exceed 60 V peak-to-peak in case of a high inductive coupling and a weak load. This signal is rectified with diodes (D1, D2) and filtered with the capacitor C_{filter} which can be seen as the energy storage for the implant. Because of such high voltage, this capacitor has been chosen with a compromise between voltage specification (50 V), capacitance value (6.8 μF), and physical dimensions. When inductive coupling is suddenly interrupted, reverse currents may occur, leading to negative voltages at the input of the first regulator (Fig.3). Diode D4 protects the circuit from such situations.

As shown in Fig.3, three linear regulators provide different power supply voltages to the neurostimulator. The first one is adjusted between 5 and 12 V for the supply of current sources and the analog supply of CMOS switches in the Stimuli Stages (Fig.4). This regulator

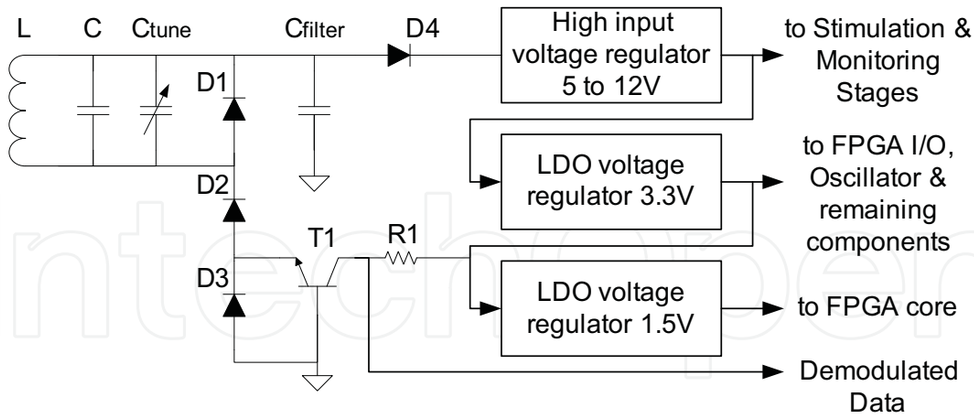

Fig. 3. Power and data recovery in UroStim8

can tolerate high input voltages up to 80 V. The second regulator provides 3.3 V that is the main supply used by the FPGA Input/Outputs buffers, the DAC, the logic supply of CMOS switches in the Stimuli Stages, and the remaining components. This regulator provides a Power-OK (POK) signal that indicates to the FPGA that the 3.3V supply is available and well regulated. No stimulation will be started unless the POK signal is high. Finally, the third supply of 1.5 V is used by the FPGA core only to reduce its power consumption.

To protect the system from a high induced voltage, power recovery circuits use voltage clipping, Zener diodes or shunt regulators (Schneider, 2001; Ba et al., 2002; Ba, 2004; Yunlei & Jin, 2005; Balachandran & Barnett, 2006). In previous neurostimulators, a shunt regulator was adjusted to be able to provide the required voltage supply in the worst case that is maximum stimulator current consumption and minimum available inductive energy. However, except in this case, it is not an efficient solution because the shunt regulator simply short-cuts the excess current. With the high input voltage of the first regulator, there is no need for voltage limiting, and the excess of inductive energy translates to voltage instead of current. Voltage is indirectly limited by the maximum available inductive energy and the minimum stimulator current consumption. Compared to the zener shunt regulator, it is a more efficient solution that also allows recovering high voltage supply for stimulation without using step-up DC/DC converters. For data recovery, the OOK demodulator is a simple envelope detector which is implemented as an amplification of small variations across diode D3 that is stacked in series between the rectifier diodes (D1, D2) and the common ground. These variations are due to the carrier modulation and are amplified with the NPN transistor T1 in a common-base configuration. A pull-up resistor R1 limits the current when the demodulated data signal is low but also limits its rising time. The design simplicity of this demodulator is the reason behind the choice of such modulation scheme for data transmission. However, the OOK modulation turns-off the coupling carrier with a duty cycle of around 50 % for each Manchester-coded bit. Consequently, inductive energy is wasted because of the simultaneous data transfer. Now that an oscillator provides a stable clock, the recovered clock is not needed anymore for stimuli generation. Thus, as soon as the FPGA acknowledges to the external controller a valid transmission, the downlink data transfer is stopped while keeping the inductive coupling. That way, more inductive energy is available for stimulation or telemetry.

3.3 Stimulation stages

UroStim8 neurostimulator has 4 stimulation stages. As presented in Fig.4, Stage 1 is dedicated to the low-frequency pulse stimulation, offers 4 bipolar outputs, and includes an 8-bit Digital to Analog Converter (DAC), an Operational Amplifier (OpAmp) used as a current source, as well as CMOS analog switches for biphasic stimulation and outputs multiplexing.

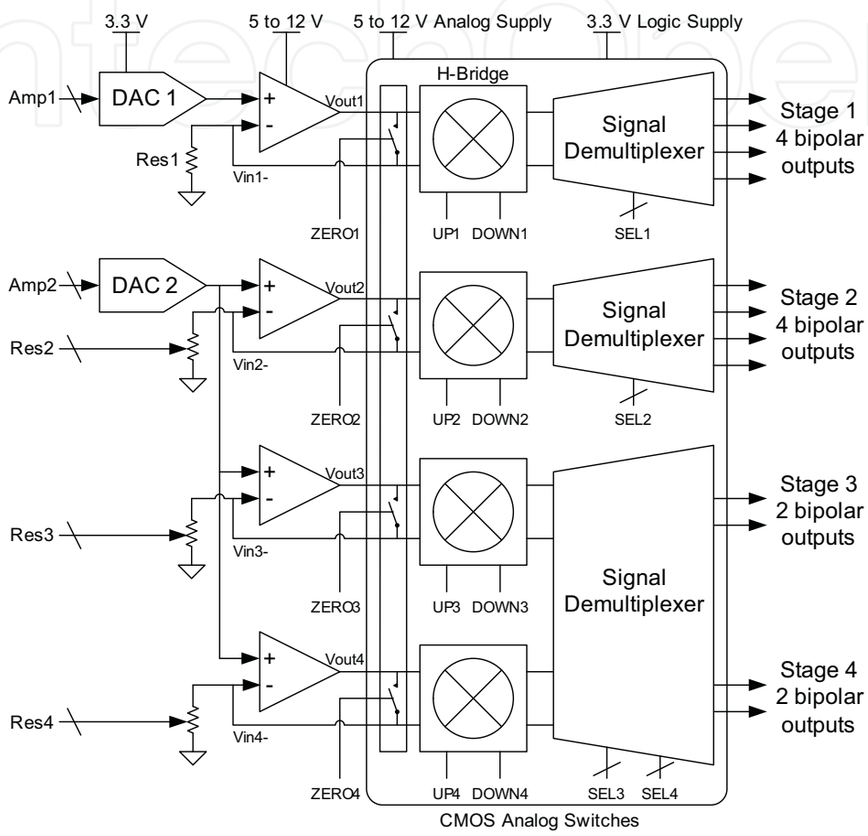

Fig. 4. Stimulation stages in UroStim8

The four outputs of Stage 1 share the same frequency and can be activated individually or in any combination. Even though meant for simultaneous stimulation, the four low-frequency pulse outputs are sequentially activated with a small delay to avoid cumulative power consumption load peaks. Thus, pulse amplitude can be programmed independently which is important because the impedance of the cuff-electrodes may be different. Before each stimulation pulse, the FPGA sends the amplitude code to the DAC that provides a proportional voltage V_{DAC} between 0 and a reference voltage of 1.2 V. This voltage is then converted into current by the OpAmp and resistance Res1 that operates as a current source. Constant current is injected into the nerve via CMOS analog switches that enables reversing the current for biphasic stimulation. The stimulation current is equal to $Istim=V_{DAC1}/Res1$, as long as the OpAmp is not saturated. Resistance Res1 has been chosen equal to 600 Ω to provide a maximum current of 2 mA (1.2 V/600 Ω). For an ENI impedance of 1 kΩ, a voltage supply of 3.3 V would have been sufficient for the OpAmp. However, previous chronic animal experiments proved that the ENI impedance may become higher than 4 kΩ

leading to lower stimulation currents because of the OpAmp saturation. Hence, its voltage supply can be increased up to 12 V so that a current of 2 mA could be injected into an ENI impedance up to 5.4 kΩ. Stimulation Stages 2 to 4 share the same DAC that will generate the sinusoidal waveform required for nerve conduction blockade. They offer 8 bipolar outputs that are grouped according to the stimulation strategy (Fig.1). For the three groups of outputs, the blockade amplitude can be adjusted independently through digital potentiometers Res2 to 4. The stimulation stages are controlled by the FPGA similarly but separately. Signals UP and DOWN sets the current direction with an H-Bridge that is made of four switches mounted as a mixer. Signal ZERO controls a fifth switch that shortcuts the OpAmp output with its negative input before activating one of the UP or DOWN signals. That way, before and after each pulse, the same voltage is applied on both electrodes (of each bipolar output) before releasing the ZERO switch (Mounaim & Sawan, 2007). The output CMOS analog switches are critical elements. If they must transmit currents under voltages as high as 12 V, they still need to be controlled by 3.3 V signals directly from the FPGA. Thus, they have been chosen with dual power supplies: a logic supply of 3.3 V and an analog supply up to 12 V.

3.4 Telemetry

The goal of the implemented telemetry is to verify the capacity of the implant to stimulate each connected nerve. Thus, it is important to monitor the load impedance presented by each ENI as it must not be too high for the desired stimulation current (Sawan et al., 2007, 2008a).

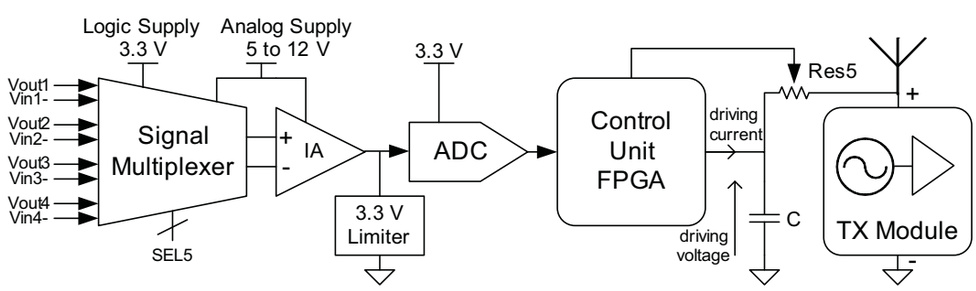

Fig. 5. Telemetry in UroStim8

The neurostimulator has a total of 12 bipolar outputs. Making use of the demultiplexers already present in the stimulation stages, monitoring can be done at the current source OpAmp output of each stage by activating one single bipolar output at a time. As shown in Fig.5, the four differential OpAmp outputs voltages are multiplexed, differentially measured with an instrumentation amplifier and then sampled with an Analog to Digital Converter (ADC) before being sent to the FPGA. The stimulus used for AC impedance measurement is a sinusoidal waveform that each stimulation stage is capable of generating. After a programmable number of cycles, the maximum amplitude and zero-crossing time of the voltage difference across the ENI, are used with the programmed stimulation parameters to estimate the impedance module and phase respectively. Once these measurements are ready, they are sent to the external controller thanks to a miniature transmission module. It is an RF emitter oscillating at 433 MHz and OOK modulated at 1 kHz. The transmission range can be adjusted with a digital potentiometer (Res5) that limits the driving current.

5. Results

The complete UroStim8 neurostimulator prototype has been assembled on a large breadboard for design and tests. Table 1 presents the achieved stimulation parameters and Fig. 6 presents different oscilloscope screen captures. Fig. 6a shows the low-frequency pulse stimulation waveform generated by Stimulation Stage 1. Single-end outputs are probed by oscilloscope channels Ch1 and Ch2 respectively. The differential output (Ch1-Ch2) is shown by the Math curve (M). Control signals ZERO1 and UP1 (according to Fig. 4) are probed by channels Ch3 and Ch4 respectively. The waveform is not a conventional biphasic one but rather an alternating monophasic waveform as proposed in (Mounaim & Sawan, 2007). Fig. 6b shows the Stimulation Stage 1 OpAmp's output Vout1 (Ch1) when all four bipolar outputs are activated. Ch2 to 4 probe three of them (single-ends only). Stimulation on the four outputs is not "truly" simultaneous but rather alternated with a small delay between pulses. This has the advantage of avoiding large current consumption peaks but also allowing different pulse amplitudes for each output. Fig. 6c and 6d show the high-frequency sinusoidal waveform at the minimum and maximum achieved frequencies respectively. For both figures, single-end outputs are probed by Ch1 and Ch2, control signals UP and DOWN (according to Fig. 4) by channels Ch3 and Ch4 respectively, while the differential output is shown by the Math curve (M).

Waveform	**Pulse**			**Sinusoid**	
Parameters	**Amp.**	**Width**	**Frequency**	**Frequency**	**Amp.**
Max	2 mA	217 µs	8.9 kHz (with min width) 1 kHz (with max width)	8.6 kHz	2 mA
Min	0	3.39 µs	18 Hz	1 kHz	0
Resolution	8 µA	Time resolution = 3.39 µs (clock = 295 kHz)			8 µA

Table 1. UroStim8 measured stimulation parameters

A normalized half-period of the waveform is stored as a map table of 1024 amplitude samples. To change the frequency of stimulation, the map table is read with a memory address step as it is scanned with the 300 kHz clock. The general equation determining the digitally programmed sinusoidal frequency is given by equation (1).

$$Frequency = 300kHz * \left(\frac{2 * 1024}{F + 7} + 5 \right)^{-1} \quad (1)$$

where F is the decimal equivalent of a programmable 6-bit binary code. As the frequency is increased, the resulting total number of amplitude steps is reduced from more than 256 (=2*1024/8) to less than 32 (=2*1024/64). Any other stimulation waveform and/or mapping strategy can be easily implemented by reprogramming the FPGA. Table 2 presents the measured system total current consumption at different conditions. With all stimulation stages and all their outputs activated, total system current consumption is 4.54 mA (rms) at 30 Hz pulse (2 mA, 217 µs) and 1 kHz sinusoidal frequencies. For Stimulation Stages 2-4, 1 mA current is distributed over outputs of each stage. Thus, stimulation parameters must be adjusted taking into account the available inductive power energy. The FPGA core current consumption in this prototype is less than 100 µA.

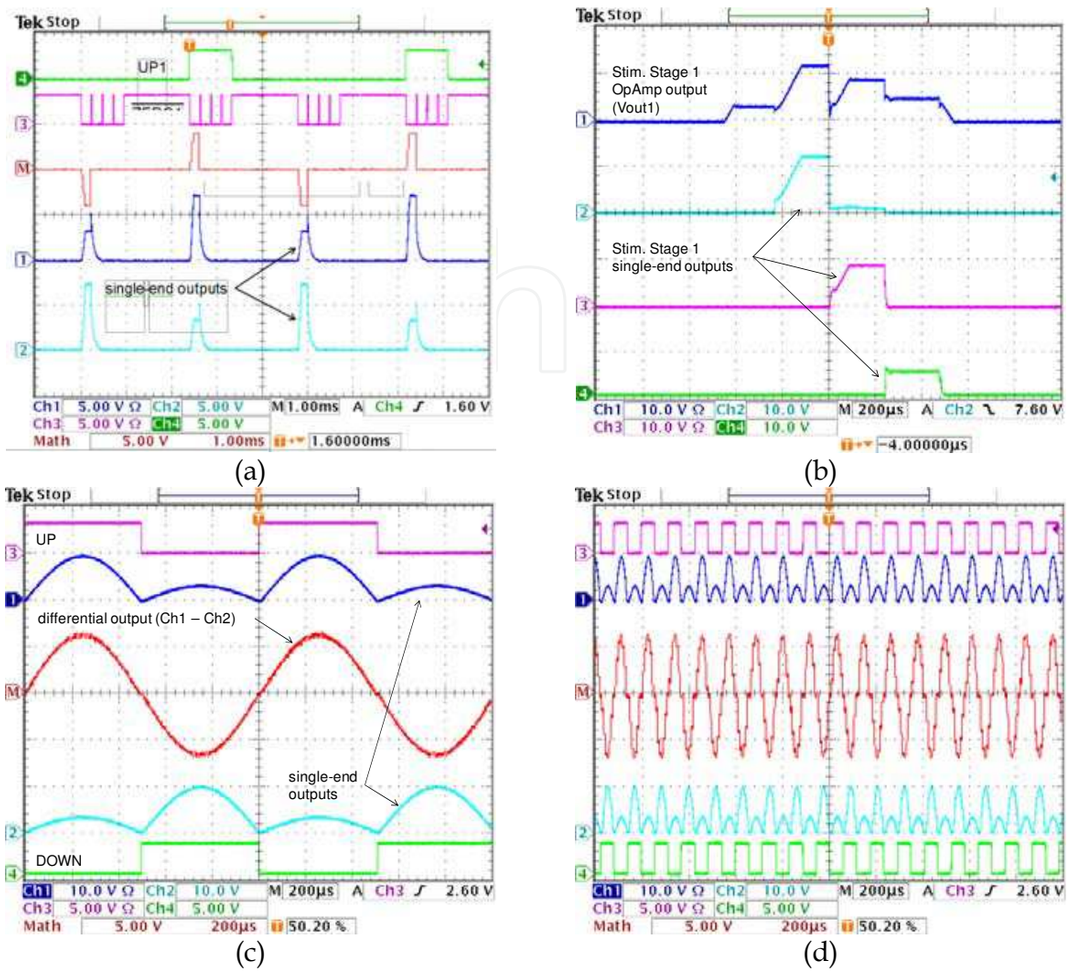

Fig. 6. Oscilloscope captures showing (a) alternating monophasic stimulation waveform and control signals, (b) Stimulation Stage 1 OpAmp output and three single-ends outputs, and sinusoidal waveform at (c) 1 kHz and (d) 8.6 kHz frequencies

Conditions		Current consumption
Stimulation Stage 1	**Stimulation Stages 2-4**	**mA (rms)**
OFF	OFF	1.83
30 Hz	OFF	2.12
1 kHz	OFF	4.59
30 Hz	1 kHz	4.54
30 Hz	8.6 kHz	5.33
1 kHz	8.6 kHz	7.80

Table 2. UroStim8 measured system total current consumption (rms) with following stimulation conditions: Stage 1 (2 mA, 217 µs); Stages 2-4 (1 mA each, current is distributed over outputs of each stage)

UroStim8 neurostimulator's printed circuit board have been designed, fabricated and assembled as shown in Fig. 7. UroStim8's PCB is 38 mm diameter and can host a FPGA in

12x12 Fine Pitch Ball Grid Array (FBGA) of 13x13 mm dimensions and 1 mm pitch. Because of the relatively large number of discrete components and the limited space, the design of such PCB is challenging. It required eight PCB layers and numerous blind vias for a complete routing of the system. For chronic animal implantation, the prototype will be encapsulated in two layers of different materials. The first layer is a rigid epoxy that protects the implant from infiltration of fluids and offers a reliable isolation for the electronic components. The second layer is a biocompatible silicone that offers a soft contact for corporal tissues. Encapsulation is done using custom made Teflon or aluminum moulds. Fig. 8 shows the targeted encapsulation dimensions for the neurostimulator. The encapsulated UroStim8 will be thinner than previous prototypes that had embedded batteries (10 mm compared to 16 mm).

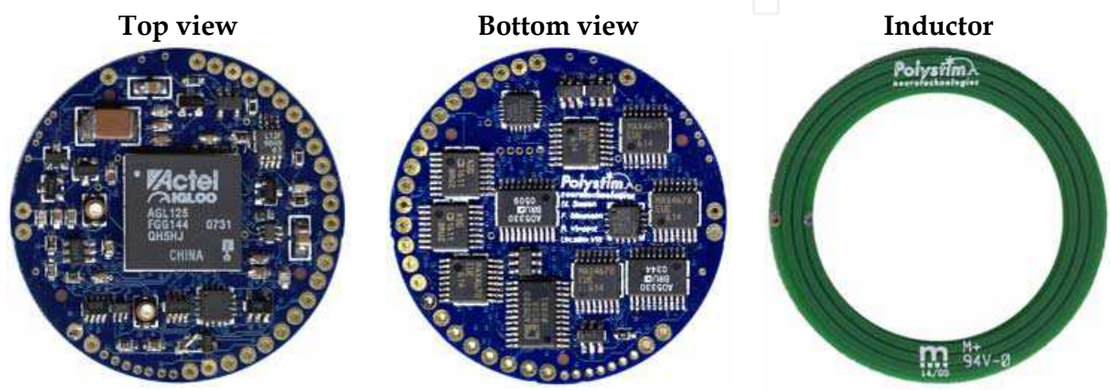

Fig. 7. UroStim8 printed circuit board

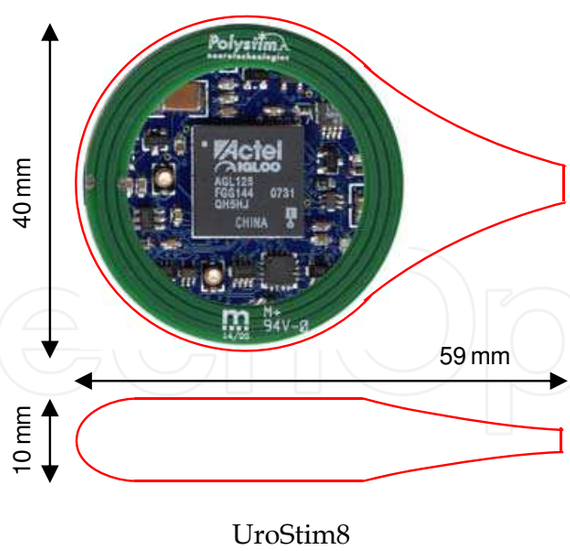

Fig. 8. UroStim8 encapsulation dimensions

6. Conclusion

This chapter presented a new sacral neurostimulation strategy to enhance micturition in spinal cord injured patients. In order to carry-on chronic animal experiments, a discrete

implantable neurostimulator has been designed implementing the proposed stimulation strategy and using commercially available discrete components. Measurements and prototyping results were presented. The discrete prototype is capable of generating a low frequency pulse waveform as low as 18 Hz with a simultaneous high frequency alternating waveform as high as 8.6 kHz, and that over different and multiple channels. With all stimulation stages and all their outputs activated, total system current consumption is around 4.5 mA (rms) at 30 Hz pulse (2 mA, 217 μs) and 1 kHz sinusoidal frequencies. In the same conditions, using a sinusoidal stimulation at the highest frequency of 8.6 kHz, increases current consumption up to 7.8 mA. With 50 mW of available inductive power for example and 4.5 mA current consumption, the high voltage regulator can be set to 10 V allowing 2 mA stimulation of 4.4 kΩ electrode-nerve impedance. However, with 7.8mA current consumption, the high voltage regulator will have to be set to 6 V reducing the maximum possible stimulation current to 1 mA for a 4.4 kΩ electrode-nerve impedance. Thus, the effective number of activated outputs and the maximum achievable stimulation parameters are limited by the available energy provided by the inductive link and the impedance of the electrode-nerve interfaces. Future developments will include chronic animal experiments after full characterization of the encapsulated and implanted neurostimulation prototype, taking into account the resulting inductive link efficiency.

7. Acknowledgement

Authors would like to acknowledge the financial support from the Natural Sciences and Engineering Research Council of Canada (NSERC), the Mycrosystems Strategic Alliance of Quebec (ReSMiQ), and the Canada Research Chair on Smart Medical Devices. Also, thanks are due to all Polystim's members and students that have participated in the design of the UroStim8 prototype and to Laurent Mouden for its assembly.

8. References

Abdel-Gawad, M.; Boyer, S.; Sawan, M. & Elhilali, M.M. (2001). Reduction of bladder outlet resistance by selective stimulation of the ventral sacral root using high frequency blockade: a chronic study in spinal cord transected dogs, *Journal of Urology*, Vol. 166, No.2, Aug. 2001, pp.728-733, 0022-5347

Ba, A.; Schneider, E.; Abdel-Karim, A.; Sawan, M. & Elhilali, M. M. (2002) Implantable dual stimulator to recuperate the bladder functions: Chronic experiments in dogs, *Int'l Functional Electrical Stimulation Society Conf.*, June 2002, IFESS, Ljubljana

Ba, A. (2004). Stimulations combinées dédiées au rétablissement de l'évacuation chez les patients souffrant de dysfonctions urinaires, M.Sc.A. dissertation, Ecole Polytechnique, Montreal (Canada), 2004.

Balachandran G. K. & Barnett, R. E. (2006). A 110 nA Voltage Regulator System With Dynamic Bandwidth Boosting for RFID Systems, *IEEE Journal of Solid-State Circuits*, Vol.41, No.9, Sept. 2006, pp.2019-2028, 0018-9200

Bhadra, N.; Kilgore, K. & Gustafson, K.J. (2006) High frequency electrical conduction block of the pudendal nerve, *Journal of Neural Engineering*, Vol.3, No.2, June 2006, pp.180-187, 2006, 1741-2560

Blaivas, J.G.; Sinha, H.P.; Zayed, A.A. & Labib, K.B. (1981). Detrusor-external sphincter dyssynergia, *Journal of Urology*, Vol.125, No.4, 1981, pp.542-544, 0022-5347

Blumer, C.E. & Quine, S. (1995). Prevalence of spinal cord injury: an international comparison, *Neuroepidemiology*, Vol.14, No.5, 1995, pp.258-68, 0251-5350

Boger, A.; Bhadra, N. & Gustafson, K.J. (2008). Bladder voiding by combined high frequency electrical pudendal nerve block and sacral root stimulation, *Neurourology and Urodynamics*, Vol.27, No.5, 2008, pp.435-439, 0733-2467

Chai, T.C. & Steers, W.D. (1996). Neurophysiology of micturition and continence, *Urologic Clinics of North America*, 1996, Vol.23, pp.221-236, 0094-0143

DeVivo, M.J. (1997). Causes and costs of spinal cord injury in the United States," *Spinal Cord*, 1997, Vol.35, No.12, pp.809-813, 1362-4393

Elabaddy, A.A.; Hassouna, M. & Elhilali M.M. (1994) Neural stimulation for chronic voiding dysfunction, *Journal of Urology*, Vol.152, 1994, pp.2076-2080, 0022-5347

Jezernik, S.; Craggs, M.; Grill, W.M.; Creasey, G. & Rijkhoff, N.J. (2002). Electrical stimulation for the treatment of bladder dysfunction: current status and future possibilities, *Neurological Research*, Vol.24, No.5, 2002, pp.413-430, 1743-1328

Kilgore, K.L. & Bhadra, N. (2004). Nerve conduction block utilising high-frequency alternating current," *Medical & Biological Engineering & Computing*, Vol.42, No.3, 2004, pp.394-406, 0140-0118

Kursun, V.; Narendra, S.G.; De, V.K. & Friedman, E.G. (2004). High input voltage step-down DC-DC converters for integration in a low voltage CMOS process, *Int'l Symp. on Quality Electronic Design*, pp.517-521, 0-7695-2093-6, Aug. 2004, IEEE, San Jose

Kutzenberger, J. (2007). Surgical therapy of neurogenic detrusor overactivity (hyperreflexia) in paraplegic patients by sacral deafferentation and implant driven micturition by sacral anterior root stimulation: methods, indications, results, complications, and future prospects, *Acta neurochirurgica Supplement*, Vol.97, No.1, 2007, pp.333-339, 0065-1419

Mounaim, F.; Sawan, M. & Bedard, S. (2006). Implantable neuro-monito-stimulation system dedicated to enhance the bladder functions, *Biomedical Circuits and Systems Conf.*, pp.198-201, 978-1-4244-0436-0, Nov. 2006, IEEE, London

Mounaim, F. & Sawan, M. (2007). Miniature Implantable System Dedicated to Bi-Channel Selective Neurostimulation, *Int'l Symp. on Circuits and Systems*, pp.2072-2075, 1-4244-0920-9, May 2007, IEEE, New Orleans

Mounaim, F.; Elzayat, E.; Sawan, M.; Corcos, J.; & Elhilali, M.M (2008). New sacral neurostimulation strategy to enhance micturition in paraplegics: Acute dog experiments, *Int'l Functional Electrical Stimulation Society Conf.*, pp.22-24, Sep. 2008, IFESS, Freiburg

Mounaim, F.; Elzayat, E.; Sawan, M.; Corcos, J.; & Elhilali, M.M (2010). New neurostimulation and blockade strategy to enhance bladder voiding in paraplegics, accepted for publication in *Contemporary Engineering Sciences*, Hikari Ltd, 1313-6569

Robin, S.; Sawan, M.; Abdel-Gawad, M.; Abdel-Baky, T.M. & Elhilali, M.M. (1998). Implantable stimulation system dedicated for neural selective stimulation, *Medical & Biological Engineering & Computing*, Vol. 36, No.4, 1998, pp.490-492, 0140-0118

Sawan, M.; Laaziri, Y.; Mounaim, F.; Elzayat, E. & Elhilali, M.M. (2007). Electrode-tissues interface: Modeling and experimental validation, *Biomedical Materials,* Vol. 2, No.1, 2007, 1748-6041

Sawan, M.; Mounaim, F. & Lesbros, G. (2008a). Wireless monitoring of electrode-tissues interfaces for long-term characterization, *Analog Integrated Circuits & Signal Processing*, Vol.55, No.1, April 2008, 0925-1030

Sawan, M.; Ba, A.; Mounaim, F.; Corcos, J. & Elhilali, M.M. (2008b). Biomedical Circuits and Systems Dedicated for Sensing and Neurostimulation: Case study on Urinary Bladder dysfunctions, *Turkish Journal of Electrical Engineering & Computer Sciences*, Vol. 16, pp.171-187, 2008, 1300-0632

Schneider, E. (2001). Conception et évaluation d'un système de stimulation électrique neurale dédié à la réhabilitation des fonctions vésicales, M.Sc.A. dissertation, Ecole Polytechnique, Montreal (Canada), 2001.

Schuettler, M.; Andrews, B.J. & Donaldson, N. de N. (2004). Blocking of Peripheral Nerve Conduction Using AC Signals: Which Frequency is Best? *Int'l Functional Electrical Stimulation Society Conf.*, pp.324-326, Sep. 2004, IFESS Bournemouth

Shaker, H.S.; Tu, L.M.; Robin, S.; Arabi, K.; Hassouna, M.; Sawan, M. & Elhilali, M.M. (1998). Reduction of bladder outlet resistance by selective sacral root stimulation using high-frequency blockade in dogs: an acute study, *Journal of Urology*, Vol.160, No.3, 1998, pp.901-907, 0022-5347

Sievert, K.D.; Gleason, C.A.; Jünemann, K.P.; Alken, P. & Tanagho, E.A. (2002). Physiologic bladder evacuation with selective sacral root stimulation: sinusoidal signal and organ-specific frequency, *Neurourology and Urodynamics*, Vol.21, No.1, 2002, pp.80-91, 0733-2467

Solomonow, M. (1984). External Control of the Neuromuscular System, *IEEE Transactions on Biomedical Engineering*, Vol.31, No.12, 1984, pp.752-763, 0018-9294

Tai, C.; de Groat, W.C. & Roppolo, J.R. (2005) Simulation analysis of conduction block in unmyelinated axons induced by high-frequency biphasic electrical currents, *IEEE Transactions on Biomedical Engineering*, Vol.52, No.7, 2005, pp.1323-1332, 0018-9294

Williamson R.P. & Andrews, B.J. (2005). Localized electrical nerve blocking, *IEEE Transactions on Biomedical Engineering*, Vol.52, No.3, 2005, pp.362-370, 0018-9294

Yunlei L. & Jin, L. (2005). A 13.56 MHz RFID transponder front-end with merged load modulation and voltage doubler-clamping rectifier circuits, *Int'l Symp. on Circuits and Systems,* Vol.5, pp.5095-5098, 0-7803-8834-8, May 2005, IEEE, Kobe

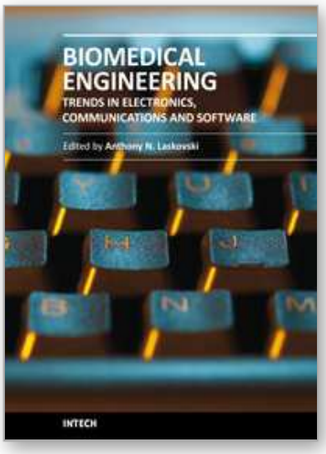

Biomedical Engineering, Trends in Electronics, Communications and Software

Edited by Mr Anthony Laskovski

ISBN 978-953-307-475-7
Hard cover, 736 pages
Publisher InTech
Published online 08, January, 2011
Published in print edition January, 2011

Rapid technological developments in the last century have brought the field of biomedical engineering into a totally new realm. Breakthroughs in materials science, imaging, electronics and, more recently, the information age have improved our understanding of the human body. As a result, the field of biomedical engineering is thriving, with innovations that aim to improve the quality and reduce the cost of medical care. This book is the first in a series of three that will present recent trends in biomedical engineering, with a particular focus on applications in electronics and communications. More specifically: wireless monitoring, sensors, medical imaging and the management of medical information are covered, among other subjects.

How to reference

In order to correctly reference this scholarly work, feel free to copy and paste the following:

Faycal Mounaim and Mohamad Sawan (2011). New Neurostimulation Strategy and Corresponding Implantable Device to Enhance Bladder Functions, Biomedical Engineering, Trends in Electronics, Communications and Software, Mr Anthony Laskovski (Ed.), ISBN: 978-953-307-475-7, InTech, Available from: http://www.intechopen.com/books/biomedical-engineering-trends-in-electronics-communications-and-software/new-neurostimulation-strategy-and-corresponding-implantable-device-to-enhance-bladder-functions

INTECH
open science | open minds

InTech Europe
University Campus STeP Ri
Slavka Krautzeka 83/A
51000 Rijeka, Croatia
Phone: +385 (51) 770 447
Fax: +385 (51) 686 166
www.intechopen.com

InTech China
Unit 405, Office Block, Hotel Equatorial Shanghai
No.65, Yan An Road (West), Shanghai, 200040, China
中国上海市延安西路65号上海国际贵都大饭店办公楼405单元
Phone: +86-21-62489820
Fax: +86-21-62489821

© 2011 The Author(s). Licensee IntechOpen. This chapter is distributed under the terms of the Creative Commons Attribution-NonCommercial-ShareAlike-3.0 License, which permits use, distribution and reproduction for non-commercial purposes, provided the original is properly cited and derivative works building on this content are distributed under the same license.